Journal of Alloys and Compounds 507 (2010) 47–52

Contents lists available at ScienceDirect

Journal of Alloys and Compounds

journal homepage: www.elsevier.com/locate/jallcom

Synthesis, electronic and magnetic properties of the double B mixed perovskite series $La_{0.5}Sr_{0.5}Mn_{1-x}Fe_xO_3$

Ganghua Zhang*, Jianhua Lin

State Key Laboratory of Rare Earth Materials Chemistry and Applications, College of Chemistry and Molecular Engineering, Peking University, Beijing 100871, China

ARTICLE INFO

Article history:
Received 4 May 2010
Received in revised form 20 July 2010
Accepted 25 July 2010
Available online 3 August 2010

Keywords:
Hydrothermal synthesis
Perovskite-type oxides
Semiconducting

ABSTRACT

The perovskite-type oxides $La_{0.5}Sr_{0.5}Mn_{1-x}Fe_xO_3$ ($x = 0.2$–0.5) were synthesized under mild hydrothermal conditions. Crystal growths of the samples were sensitive to the Mn-containing precursor, alkalinity and the reaction temperature. All the compounds corresponded to orthorhombic structure of space group *Pnma*. The curves *M* vs. *T* for the compositions with $x = 0.2$, 0.3 and 0.4 indicated the coexistence of ferro- and anti-ferromagnetic contribution. The temperature dependence $\rho(T)$ is semiconducting for all the compounds and explained well by the variable range hopping rather than the adiabatic small polaron hopping.

1. Introduction

The colossal magnetoresistance (CMR) manganites $La_{1-x}A_xMnO_3$ ($A^{2+} = Ca^{2+}$, Sr^{2+}, Ba^{2+}, Pb^{2+}) have attracted worldwide attention because of their extraordinary electrical and magnetic properties and their future potential in technological applications [1,2]. The substitution of the Mn ions by other transition metal ion, such as Cr, Fe, Co and Ni, can give rise to important modifications in the magnetic and transport properties [3–8]. Among others, Fe is particularly interesting, because it does not cause considerable lattice distortion [9] due to close ionic radii of Fe^{3+} and Mn^{3+} [10], which is a special model to study the unique properties of manganites. As the Mn atoms are substituted by Fe the magnetic structure dramatically changes: the charge order (CO) phenomenon is disrupted for low Fe concentration and the larger the Fe content, the lower the Curie temperature and the magnetic moment per Mn/Fe atom, because the ferromagnetic double-exchange chain is broken [11–13].

The conventional syntheses for the Fe-doped manganites are through high-temperature solid-state reactions between oxides, nitrates and/or carbonate precursors [9–14]. But it needs much higher temperature, and the inhomogeneous chemical components and the multiphase of the sample usually cannot be avoided. However, for the advantages of the lower reaction temperature and simple apparatus, hydrothermal process has been employed to synthesize the oxide powders of high purity, narrow particle-size distribution, high phase homogeneity, controlled particle morphology and a high degree of crystallinity. The partial substitution in A-site of perovskite manganates has been achieved under hydrothermal conditions [15]. To the best of our knowledge, there are no reports on the hydrothermal synthesis of the manganites with other transition metal elements doping on Mn site. Moreover, although there are already some reports on the Fe-doped $La_{1-x}Sr_xMnO_3$ systems by solid-state reactions [7,16], the effect of Fe doping on the $La_{0.5}Sr_{0.5}MnO_3$ has not been reported on a systematic study. Therefore we explored the applicability of hydrothermal synthesis of the partial substitution in B-site of $La_{0.5}Sr_{0.5}MnO_3$ by Fe. In this paper, we reported a series of the perovskite-type oxides of the formula $La_{0.5}Sr_{0.5}Mn_{1-x}Fe_xO_3$ ($x = 0.2$–0.5) synthesized under mild hydrothermal conditions. We also investigated the effect of Fe substitution on magnetic and electrical properties.

2. Experimental section

In a typical synthesis procedure for $La_{0.5}Sr_{0.5}Mn_{0.5}Fe_{0.5}O_3$, 5.75 ml $KMnO_4$ (0.1 M) and 10 g KOH were mixed by stirring to form a solution. To this solution, we added 9.63 ml $MnCl_2$ (0.2 M) dropwise on stirring and cooled in an ice bath to form k-birnessite gel precursor. This was followed by an addition of 12.5 ml $Sr(NO_3)_3$ (0.2 M), 12.5 ml $La(NO_3)_3$ (0.2 M), 12.5 ml $Fe(NO_3)_3$ (0.2 M) and 60 g KOH. The reaction mixture was then transferred into an 80-ml Teflon-lined stainless steel autoclave with a filling capacity of 80%. The crystallization was carried out under autogenous pressure at 260 °C for 3 days. After the autoclave was cooled and depressurized, the products were washed with distilled water and sonicated by a direct immersion of a titanium horn (Vibracell, 20 kHz, 200 W/cm^2). And then, single-phase $La_{0.5}Sr_{0.5}Mn_{0.5}Fe_{0.5}O_3$ was obtained as a fine dark crystalline powder at the bottom of the beaker. The reaction conditions employed for the synthesis of other compositions are listed in Table 1. The reaction equation for the synthesis of $La_{0.5}Sr_{0.5}Mn_{0.5}Fe_{0.5}O_3$ can be proposed as below:

* Corresponding author. Tel.: +86 10 62763392; fax: +86 10 62751708.
E-mail address: ganghuazhang@pku.edu.cn (G. Zhang).

0925-8388/$ – see front matter © 2010 Elsevier B.V. All rights reserved.
doi:10.1016/j.jallcom.2010.07.162

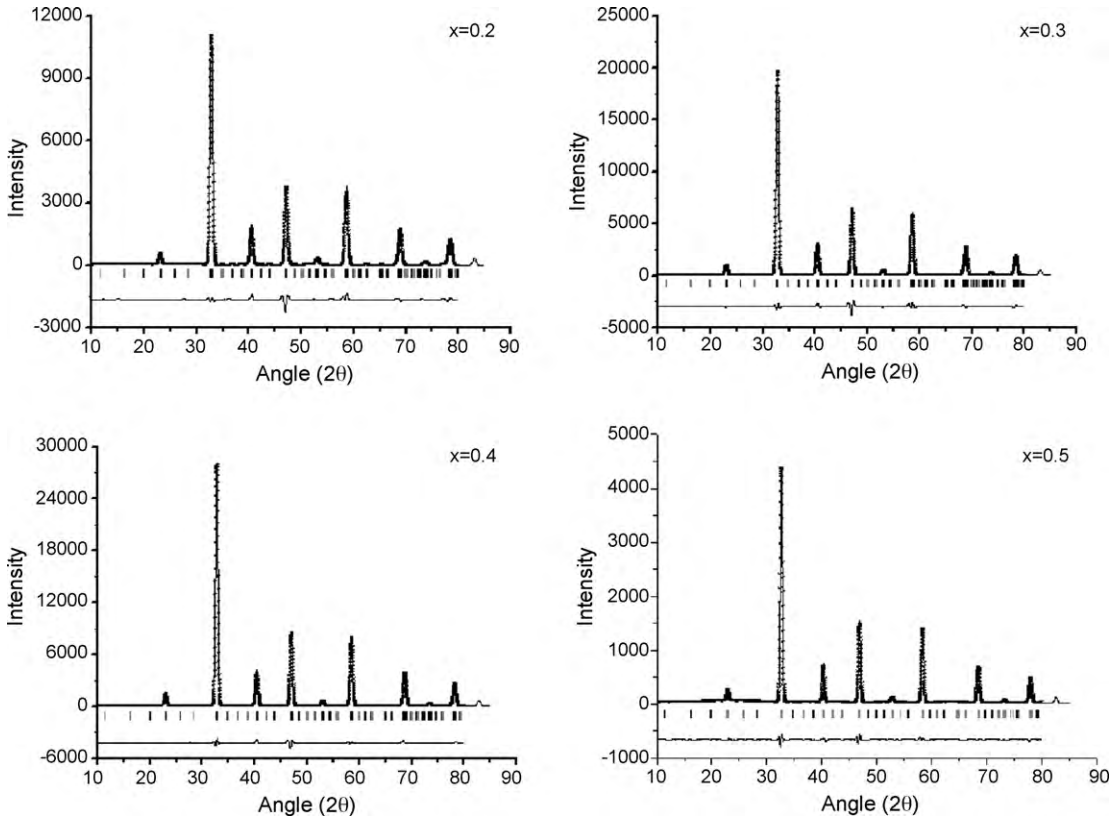

Fig. 1. The experimental, calculated and difference X-ray diffraction profiles for $La_{0.5}Sr_{0.5}Mn_{1-x}Fe_xO_3$ (x = 0.2, 0.3, 0.4 and 0.5).

Table 1
The optimal synthetic conditions for preparing $La_{0.5}Sr_{0.5}Mn_{1-x}Fe_xO_3$ (x = 0.2, 0.3, 0.4 and 0.5).

x	Molar ratio of initial reagents $n(La^{3+}):n(Sr^{2+}):n(M)^a:n(Fe^{3+})$	Calculated value from ICP ($n_{La}:n_{Sr}:n_{Mn}:n_{Fe}$)	Alkalinity (M)	Reaction temperature (°C)
0.5	0.50:0.50:0.50:0.50	0.52:0.48:0.51:0.49	19	260
0.4	0.50:0.50:0.60:0.40	0.51:0.49:0.62:0.38	18	260
0.3	0.50:0.50:0.70:0.30	0.50:0.50:0.72:0.28	15	260
0.2	0.50:0.50:0.80:0.20	0.51:0.49:0.81:0.19	15	260

[a] $n(M) = n(MnO_4^-) + n(Mn^{2+})$; $n(MnO_4^-)/n(Mn^{2+}) = 0.3$.

$$0.5La^{3+} + 0.5Sr^{2+} + 0.5Fe^{3+} + 0.5K_xMnO_2 + 0.125xO_2 + (4 - 0.5x)OH^- \rightarrow La_{0.5}Sr_{0.5}Mn_{0.5}Fe_{0.5}O_3 + 0.5xK^+ + (2 - 0.25x)H_2O$$

Powder X-ray diffraction (XRD) data were collected by a Rigaku D/Max 2500V/PC X-ray diffractometer using Cu$K\alpha$ radiation (λ = 1.5418 Å) at 50 kV and 250 mA. Scanning electron microscopy (SEM) was performed on a Rigaku JSM-6700F microscope operating at 10 kV. Inductively couple plasma (ICP) analysis was carried out on a Perkin-Elmer Optima 3300DV ICP instrument. The average B-site oxidation state of the powders was determined by iodometric titrations. The ^{57}Fe Mössbauer spectra were recorded by a constant acceleration Mössbauer spectrometer with a ^{57}Co(Pd) source at room temperatures.

Table 2
Unit cell, positional and reliability factors for the Rietveld refinements of $La_{0.5}Sr_{0.5}Mn_{1-x}Fe_xO_3$ (x = 0.2, 0.3, 0.4 and 0.5), in the orthorhombic *Pnma* space group from XRD data.

x		0.5	0.4	0.3	0.2
a (Å)		5.478 (8)	5.482 (1)	5.441 (1)	5.428 (1)
b (Å)		7.762 (2)	7.717 (1)	7.692 (1)	7.672 (1)
c (Å)		5.479 (7)	5.461 (1)	5.479 (1)	5.465 (1)
v (Å^3)		232.9 (7)	231.0 (3)	229.3 (1)	227.5 (8)
R/Sr 4c (x, y, 1/4)	x	0.00049 (7)	−0.00005 (2)	0.00127 (3)	−0.00088 (6)
	y	−0.00064 (1)	−0.00241 (7)	0.00131 (5)	−0.00420 (5)
Mn/Fe 4b (0, 0, 1/2)					
O1 4c (x, y, 1/4)	x	0.5191 (3)	0.5013 (1)	0.5426 (8)	0.5505 (4)
	y	−0.0022 (6)	−0.0055 (6)	0.0317 (1)	0.0097 (1)
O2 8d (x, y, z)	x	0.2191 (2)	0.2593 (6)	0.2331 (7)	0.2359 (3)
	y	0.0177 (5)	0.0006 (8)	0.0004 (2)	0.0059 (5)
	z	0.7785 (5)	0.7608 (8)	0.7649 (9)	0.7610 (8)
R_{wp} (%)		10.45	8.80	11.94	11.59
R_p (%)		6.44	4.58	6.73	6.56
χ^2		1.57	1.15	1.17	1.14

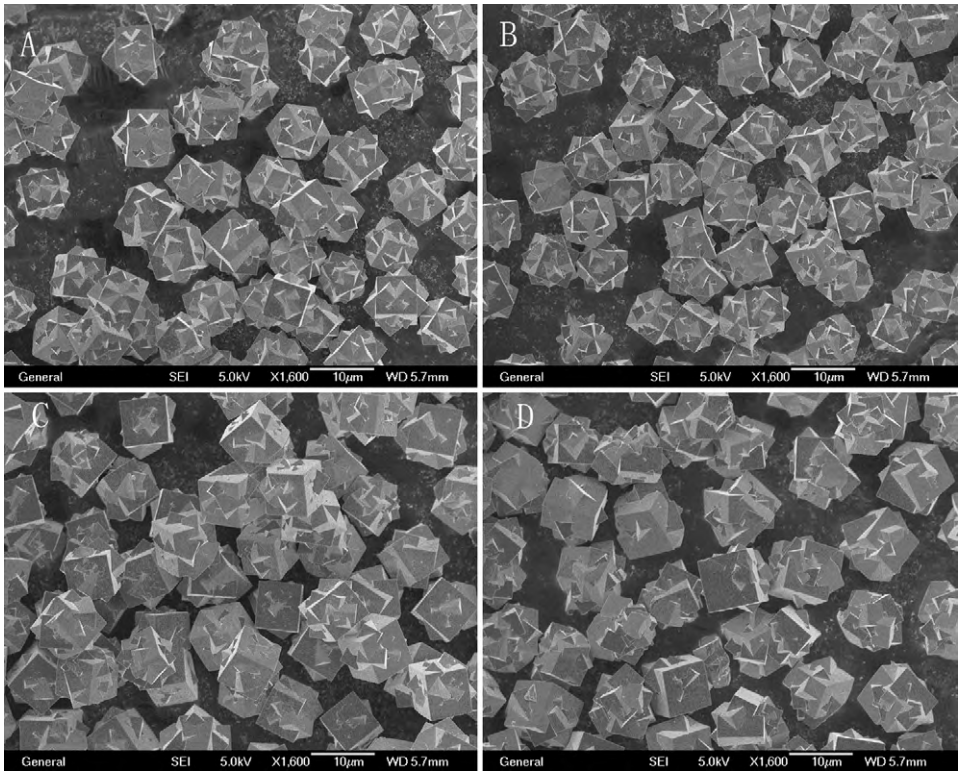

Fig. 2. SEM images of crystalline samples. (A): $x = 0.5$; (B): $x = 0.4$; (C): $x = 0.3$; and (D): $x = 0.2$.

The magnetic properties of the $La_{0.5}Sr_{0.5}Mn_{1-x}Fe_xO_3$ were studied using a superconducting quantum interference device magnetometer (Quantum Design, MPMS). The DC susceptibility measurements, both under zero-field-cooling (ZFC) and field-cooling (FC) conditions, were performed in a 100 Oe magnetic field for temperatures ranging from 4 to 300 K. The temperature variation of the resistivity, $\rho(T)$, was measured using the standard four-probe technique collected on a quantum design physical properties measurement system (PPMS).

3. Results and discussion

In the hydrothermal process, there are many influencing factors for the crystal growth of our samples. Among these, the Mn-containing precursor (k-birnessite), alkalinity and the reaction temperature are critical factors. For the strong activity in hydrothermal condition, the birnessites has been reported as a good synthetic precursor to porous manganese oxide octahedral molecular sieve (OMS), which has interesting structural, catalytic, electrical and adsorptive properties [17,18]. In this work, the k-birnessite prepared by the already reported method [19], acted as a synthetic precursor to the target products. The optimal ratio range of MnO_4^-/Mn^{2+} to form the k-birnessite is 0.25–0.4 [20]. Here we chose the ratio of 0.3 to obtain the k-birnessite. Interestingly, we can adjust the doping level (x) in $La_{0.5}Sr_{0.5}Mn_{1-x}Fe_xO_3$ only by changing the appropriate ratio of Mn/Fe. This is unlike reported in A-site substitution that the adjustment of the MnO_4^-/Mn^{2+} ratio is required to obtain different compositions [15]. Besides the precursor, it has been found that the compound cannot be obtained when the reaction temperature is lower than 260 °C due to the formation of $La(OH)_3$ and $Fe(OH)_3$. KOH not only maintains the alkalinity but also acts as mineralizing agent. The high alkalinity of the reaction system is necessary, because it considerably influences the crystallization of $La_{0.5}Sr_{0.5}Mn_{1-x}Fe_xO_3$. If the alkalinity is less than 10 M, a powder mixture of $La(OH)_3$, $K_xMnO_2{\cdot}0.5–0.7H_2O$ and $Fe(OH)_3$ was fabricated and the crystallization degree is not very good. But we cannot obtain the composition with the x value higher than 0.5. This is maybe due to the reason of the special synthesis method for higher valence of Fe. If $x > 0.5$, the oxidation state of Fe should be higher than +3. Usually the perovskite-type oxides with higher Fe valence can be obtained by solid-state reactions [21,22]. EDX analysis of selected regions for the sample showed the presence of all four metals in area analyzed with a constant ratio. The ICP analysis revealed a nominal ratio of La, Sr, Mn, Fe shown in Table 1. The oxygen contents in our samples obtained from iodometric titration approached to 3.

The room-temperature powder X-ray diffraction patterns for $La_{0.5}Sr_{0.5}Mn_{1-x}Fe_xO_3$ ($x = 0.2$, 0.3, 0.4 and 0.5) are shown in Fig. 1. The XRD data could be indexed on the basis of known perovskite $GdFeO_3$ crystal structure [23] and refined by the Rietveld method. The products crystallize in the orthorhombic system

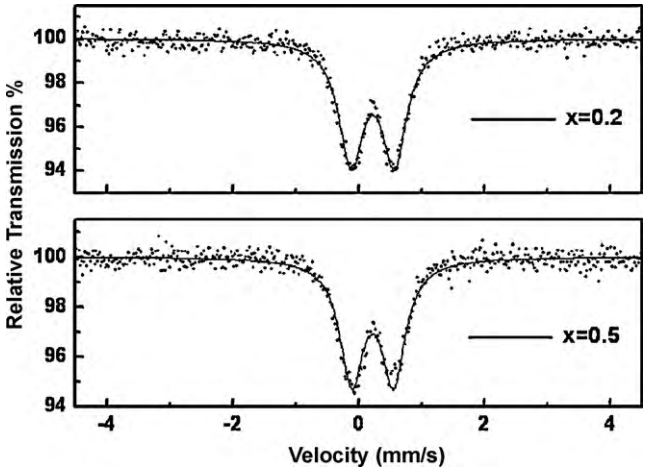

Fig. 3. Mössbauer spectra of $La_{0.5}Sr_{0.5}Mn_{1-x}Fe_xO_3$ at room temperature ($x = 0.5$ and 0.2).

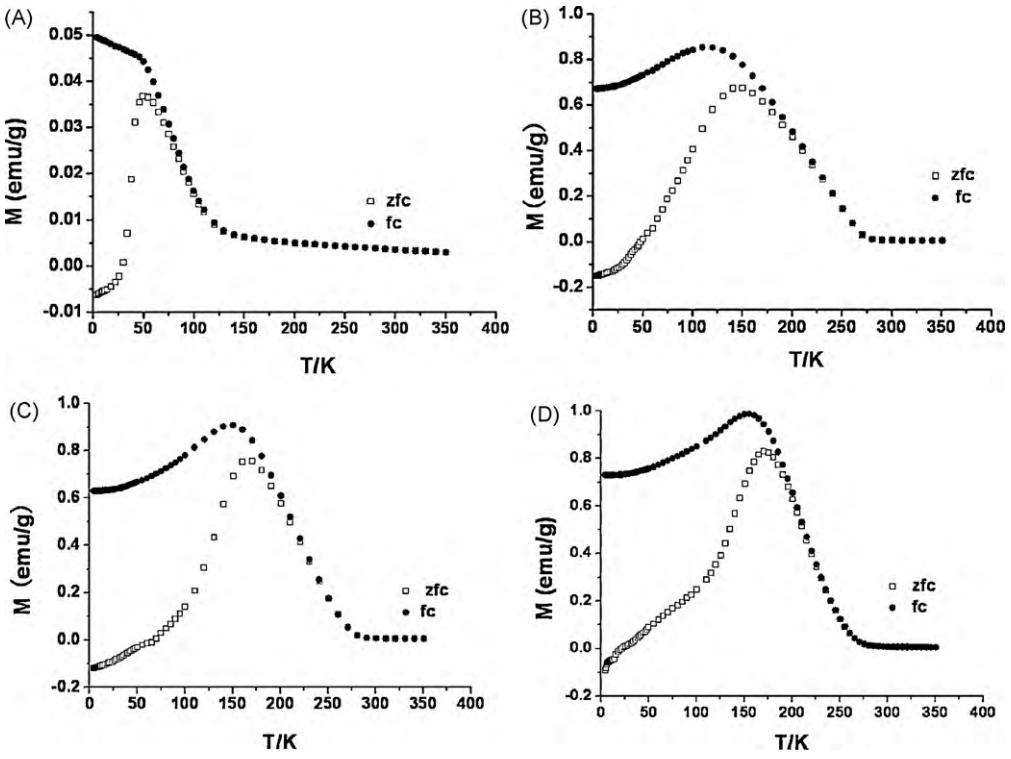

Fig. 4. Zero-field-cooled (ZFC) and field-cooled (FC) magnetization curves of $La_{0.5}Sr_{0.5}Mn_{1-x}Fe_xO_3$ obtained by hydrothermal synthesis with the applied field of 100 Oe. (A): $x = 0.5$; (B): $x = 0.4$; (C): $x = 0.3$; and (D): $x = 0.2$.

with space group *Pnma*. The crystallographic parameters for $La_{0.5}Sr_{0.5}Mn_{1-x}Fe_xO_3$ are listed in the Table 2. As shown in Table 2, the unit cell volume slightly decreases as the iron content decrease, which is consistent with the size differences between the Mn^{3+} and Fe^{3+} ions. In fact, the ionic size of Fe^{3+} is 0.645 Å whereas that of Mn^{3+} is 0.64 Å; hence the substitution of Fe^{3+} should not introduce noticeable lattice distortion. Similar findings have been observed by other researchers also [8,24]. The twinned crystallization of the products obtained by hydrothermal synthesis was observed by SEM image shown in Fig. 2. SEM photographs of the samples show clearly the materials to be made up from unique star-like small crystallites, around 10 μm in a narrow particle-size distribution.

In order to detect the valence states of manganese and iron, we measured their average valences by iodometry. The experimental average valence state of B-site is +3.47 to +3.49, very close to the theoretical value of 3.5 calculated from the neutrality for the title compounds. The oxidation state of Fe in the different samples was identified by Mössbauer spectra. Fig. 3 shows the ^{57}Fe Mössbauer spectrum at room temperature for two representative compositions with $x = 0.5$ and 0.2. In all cases, the spectrum exhibits a doublet pattern indicating the paramagnetic state of the samples at room temperature. The isomer shifts for $x = 0.5$ and 0.2 are found to be 0.36 mm/s. These values are typical of Fe^{3+} ions in octahedral coordination, being in accordance with previous works [25,26]. Therefore, the oxidation state of Fe in our samples is +3 whereas Mn is a mixed valence of Mn^{3+}/Mn^{4+}.

In Fig. 4 we show the temperature dependence of the zero-field-cooled (ZFC) and field-cooled (FC) magnetization at a magnetic field of 100 Oe for the series $La_{0.5}Sr_{0.5}Mn_{1-x}Fe_xO_3$ compounds. ZFC curves ($x = 0.2$, 0.3, 0.4 and 0.5) show that the M value initially increases gradually with the decrease of temperature, and then drops remarkably at $T_f \sim 170$, 165, 150 and 50 K, respectively. (T_f is defined as spin frozen temperature.) All the ZFC curves do not coincide with FC curves just below T_f. The zero-field-cooling (ZFC)–field cooling (FC) curves indicate a large inhomogeneity of the magnetic distribution for all the compounds. For all the samples, ZFC magnetization exhibited negative polarity. This can be understood in terms of random orientation of magnetic domains after zero-field-cooling.

The curves M vs. T for the compositions with $x = 0.2$, 0.3 and 0.4 indicated the existence of ferro- and anti-ferromagnetic contribution at lower temperature. And this is consistent with the previously reported in the La–Sr–Mn–Fe–O systems [7,16]. Fig. 5 shows the isothermal magnetization curves of all the compounds studied here. From the plots it is clear that the FM phase was observed in samples with all doping level ($0.2 \leq x \leq 0.5$). It is also clear that the highest magnetic field of 5 T (the highest in our SQUID magnetometer) is too low to saturate the magnetization. A small hysteresis is observed in all of title compounds

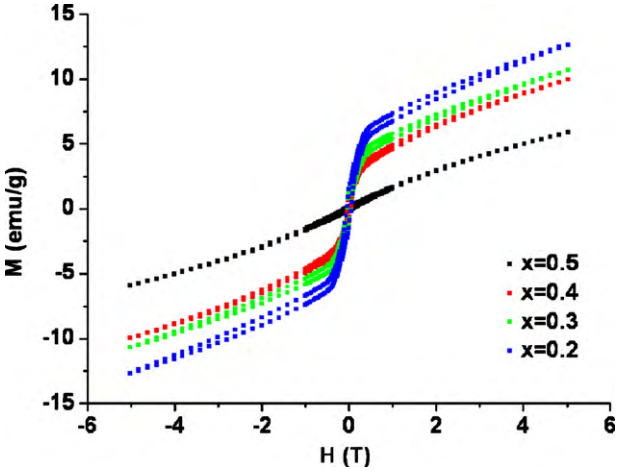

Fig. 5. Isothermal magnetization curves of $La_{0.5}Sr_{0.5}Mn_{1-x}Fe_xO_3$ ($x = 0.5$, 0.4, 0.3 and 0.2) at 4 K.

at low temperatures. For $x = 0.5$, the weak ferromagnetic property can reasonably be explained in terms of slight canted spin arrangement. With decreasing of x, the amount of Mn^{3+} ions simultaneously increased for the valence balance. As a result, a typical double-exchange interaction occurs due to the existence of mixed valence Mn^{3+}/Mn^{4+} in this system, which induces the appearance of FM phase in AFM background. Therefore, the coexistence of the FM and AFM interactions was observed in the present system. As previously reported, the introduction of Fe in the samples causes an important decrease in the temperature of ferromagnetic ordering [27,28], following the same behavior observed for the insulator–metal transition [29]. And it can be also observed in our system that the presence of Fe favors a negative contribution to the double-exchange mechanism. With the decreasing of the Fe content, the maximum in the ZFC magnetizations curve displayed an obviously increasing. Same orderliness also can be found in Fig. 5.

Fig. 6 displays the temperature-dependent resistivity of the four compounds measured from 5 to 300 K without applying magnetic field. With decreasing x, the absolute value decreases nearly exponentially as seen in the $\ln\rho$ (200 K) vs. T plot in the inset of Fig. 6 (also Fig. 7). This is because of the enhanced Mn^{3+}–O–Mn^{4+} double-exchange interaction due to the increasing content of Mn^{3+} ions. Obviously, the double-exchange interaction is in favor of electronic transport. For all the samples, the temperature dependence of resistivity exhibits a semiconducting behavior. Generally, two models have been employed to describe the semiconducting transport. One is small polaron hopping (SPH) model: $\rho(T)$ is expressed as $\rho(T)/T \propto \exp(E_P/k_BT)$); Ep being the activation energy [30]. The other one is variable range hopping (VRH) model: $\rho(T)$ is expressed as $\rho(T) \propto \exp(T_0/T)^{1/4}$; T_0 being the characteristic temperature [31]. Here, $\rho(T)$ was analyzed using both VRH and SPH models, which are shown in Fig. 7. The comparison of these two fitting results exhibits that the VRH model shows better for $x \leq 0.4$ samples whereas $\rho(T)$ follows the SPH model only in high-temperature regions. For $x = 0.5$ the temperature range of the measurement is not sufficient to compare the data with the models. In the present system, Fe^{3+} ion acted as an impurity which induces the formation of a random magnetic phase and weakens the double-exchange interaction. The e_g electron has to hop between the clusters or domains resulting in a semiconducting behavior. Therefore, the transport properties of our samples can be depicted better by the VRH model. Moreover, the VRH conduction mechanism has also been observed in other Fe-doped manganites [32,33].

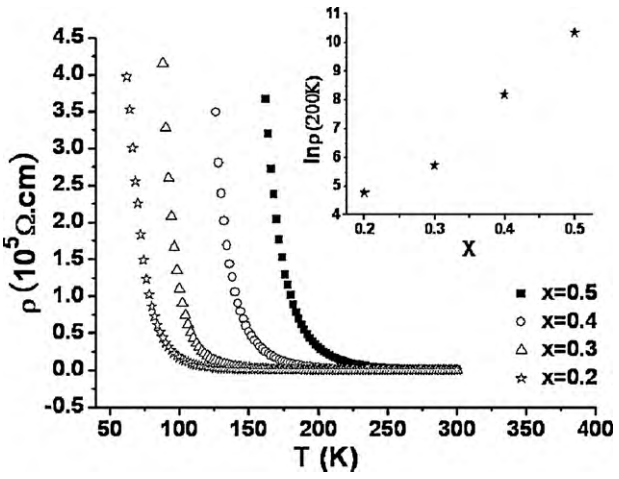

Fig. 6. Temperature variation of the resistivity for $La_{0.5}Sr_{0.5}Mn_{1-x}Fe_xO_3$ with $x = 0.5$, 0.4, 0.3 and 0.2. The inset shows the semi-logarithmic plot of ρ at 200 K against x.

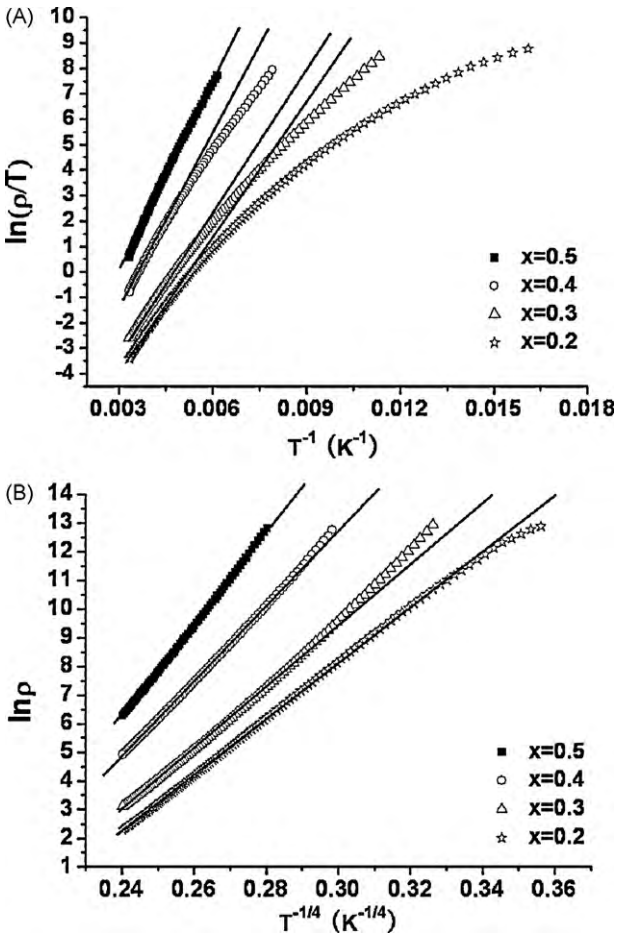

Fig. 7. The plot of (A) $\ln(\rho/T)$ vs. $1/T$ and (B) $\ln\rho$ vs. $T^{-1/4}$ for $La_{0.5}Sr_{0.5}Mn_{1-x}Fe_xO_3$ with $x = 0.5$, 0.4, 0.3 and 0.2. The straight lines indicate the fitting to the SPH and VRH models.

4. Conclusion

In the present studies, a series of the perovskite-type oxides $La_{0.5}Sr_{0.5}Mn_{1-x}Fe_xO_3$ ($x = 0.2$, 0.3, 0.4 and 0.5) have been synthesized by hydrothermal reaction technique and the crystal has a uniform size about 10 μm. The Mn-containing precursor (kbirnessite), alkalinity and the reaction temperature are found to be critical factors that influence the crystallization of the samples. The curves M vs. T for the compositions with $x = 0.2$, 0.3 and 0.4 present the coexistence of ferro- and anti-ferromagnetic. The resistivity shows semiconducting features for all the compounds. The electronic transport of our samples prefers to realize by the VRH manner rather than the SPH one. Our study indicated that the hydrothermal method is another route to the synthesis for more complicated perovskite-type oxides.

References

[1] S. Jin, T.H. Tiefel, M. McCormack, R.A. Fastnacht, R. Ramesh, L.H. Chen, Science 264 (1994) 413.
[2] R.V. Helmolt, J. Wecker, B. Holzapfel, L. Schultz, K. Samwer, Phys. Rev. Lett. 71 (1993) 2331.
[3] I.D. Fawcett, G.M. Veith, M. Greenblatt, M. Croft, I. Nowik, Solid State Sci. 2 (2000) 821.
[4] F. Rivadulla, M.A. López-Quintela, L.E. Hueso, P. Sande, J. Rivas, R.D. Sanchez, Phys. Rev. B 62 (2000) 5678.
[5] S.L. Young, Y.C. Chen, H.Z. Chen, L. Horng, J.F. Hsueh, J. Appl. Phys. 91 (2002) 8915.
[6] H. Song, W. Kim, S.J. Kwon, J. Kang, J. Appl. Phys. 89 (2001) 3398.
[7] K. Ramesha, V. Thangadurai, D. Sutar, S.V. Subramanyam, G.N. Subbanna, J. Gopalakrishnan, Mater. Res. Bull. 35 (2000) 559.

[8] Y. Ying, N.V. Dai, T.W. Eom, Y.P. Lee, J. Appl. Phys. 105 (2009) 093924.
[9] K.H. Ahn, X.W. Wu, K. Liu, C.L. Chien, Phys. Rev. B 54 (1996) 15299.
[10] R.D. Shannon, Acta Crystallogr. A 32 (1976) 751.
[11] J. Gutiérrez, A. Peña, J.M. Barandiarán, J.L. Pizarro, T. Hernández, L. Lezama, M. Insausti, T. Rojo, Phys. Rev. B 61 (2000) 9028.
[12] B. Hannoyer, G. Marest, J.M. Greneche, R. Bathe, S.I. Patil, S.B. Ogale, Phys. Rev. B 61 (2000) 9613.
[13] A. Simopoulos, M. Pissas, G. Kallias, E. Devlin, N. Moutis, I. Panagiotopoulos, D. Niarchos, C. Christides, R. Sonntag, Phys. Rev. B 59 (1999) 1263.
[14] P. Levy, L. Granja, E. Indelicato, D. Vega, G. Polla, F. Parisi, J. Magn. Magn. Mater. 226 (2001) 794.
[15] Y. Chen, H. Yuan, G. Tian, G. Zhang, S. Feng, J. Solid State Chem. 180 (2007) 167.
[16] D.C. Kundaliya, R. Vij, R.G. Kulkarni, A.A. Tulapurkar, R. Pinto, S.K. Malik, W.B. Yelon, J. Magn. Magn. Mater. 264 (2003) 62.
[17] Y.F. Shen, R.P. Zerger, R.N. DeGuzman, S.L. Suib, L. McCurdy, D.I. Potter, C.L. O'Young, Science 260 (1993) 511.
[18] Y.H. Xu, Q. Feng, K. Kajiyoshi, K. Yanagisawa, Chem. Mater. 14 (2002) 697.
[19] X.F. Shen, Y.S. Ding, J. Liu, J. Cai, K. Laubernds, R.P. Zerger, A. Vasiliev, M. Aindow, S.L. Suib, Adv. Mater. 17 (2005) 805.
[20] J. Luo, Q. Zhang, S.L. Suib, Inorg. Chem. 39 (2000) 741.
[21] Y. Liang, N. Di, Z. Cheng, Phys. Rev. B 72 (2005) 134416.
[22] Y. Liang, N. Di, Z. Cheng, J. Magn. Magn. Mater. 306 (2006) 35.
[23] M. Marezio, J.P. Remeika, P.D. Dernier, Acta Crystallogr. B 26 (1970) 2008.
[24] V. Dayal, S. Keshri, Solid State Commun. 142 (2007) 63.
[25] F.M.A. Da Costa, A.J.C. Dos Santos, Inorg. Chim. Acta 140 (1987) 105.
[26] T. Hernández, F. Plazaola, T. Rojo, H.M. Barandiaran, J. Alloys Compd. 323–324 (2001) 440.
[27] K.H. Ahn, X.W. Wu, C.L. Chien, J. Appl. Phys. 81 (1997) 5505.
[28] A. Ajan, N. Venkateramani, S. Prasad, S.N. Shringi, A.K. Nigam, R. Pinto, J. Appl. Phys. 83 (1998) 7169.
[29] A. Tiwari, K.P. Rajeev, J. Appl. Phys. 86 (1999) 5175.
[30] N.F. Mott, E.A. Davis, Electrical Process in Non-Crystalline Materials, Clarendon, Oxford, 1971.
[31] N.F. Mott, J. Non-Cryst. Solids 1 (1968) 1.
[32] M. Viret, L. Ranno, J.M.D. Coey, Phys. Rev. B 55 (1997) 8067.
[33] L. Pi, L. Zheng, Y.H. Zhang, Phys. Rev. B 61 (2000) 8917.